Acceleration of Perfusion MRI Using Locally Low-Rank Plus Sparse Model

Marie Daňková[1,2], Pavel Rajmic[1], and Radovan Jiřík[3]

[1] SPLab, Brno University of Technology, Brno, Czech Republic
m.dankova@phd.feec.vutbr.cz, rajmic@feec.vutbr.cz
[2] CEITEC, Masaryk University, Brno, Czech Republic
[3] ASCR, Institute of Scientific Instruments, Brno, Czech Republic
jirik@isibrno.cz

Abstract. Perfusion magnetic resonance imaging is a technique used in diagnostics and evaluation of therapy response, where the quantification is done by analyzing the perfusion curves. Perfusion- and permeability-related tissue parameters can be obtained using advanced pharmacokinetic models, but, these models require high spatial and temporal resolution of the acquisition simultaneously. The resolution is usually increased by means of compressed sensing: the acquisition is accelerated by under-sampling. However, these techniques need to be improved to achieve higher spatial resolution and/or to allow multislice acquisition. We propose a modification of the L+S model for the reconstruction of perfusion curves from the under-sampled data. This model assumes that perfusion data can be modelled as a superposition of locally low-rank data and data that are sparse in the spectral domain. We show that our model leads to a better performance compared to the other methods.

Keywords: perfusion, MRI, DCE-MRI, compressed sensing, sparsity, locally low-rank

1 Introduction

Perfusion magnetic resonance imaging (MRI), more specifically the dynamic contrast enhanced MRI (DCE-MRI) [1–4], is nowadays a promising method for medical diagnosis and evaluation of therapy response. Using perfusion MRI, oncological and cardiovascular diseases can be diagnosed and their effective treatment can be monitored. In perfusion MRI, a suitable contrast agent is administered intravenously. Due to the cardiovascular system, the contrast agent is distributed within the organism and its temporal and spatial distribution can be observed and analyzed. The time dependency of contrast agent concentration in a region of interest is called *perfusion curve(s)*. The tissue-specific perfusion parameters, necessary for the diagnosis, are estimated from the perfusion curves by approximation using a pharmacokinetic model.

The usual pharmacokinetic models in use are the Tofts and the extended Tofts models [5], which only allow estimating of a limited number of perfusion

parameters. To allow estimating of additional highly relevant perfusion parameters such as the blood flow and vessel permeability, more complex models need to be used [5]. However, successful application of such models assumes high temporal resolution of the acquisition to capture the vascular-distribution phase of the contrast agent. These requirements substantially limit the achievable spatial resolution of the data acquired or the ability to acquire multiple slices (i.e. perfusion curves in 3D volume). Using the classic (Nyquist-rate) acquisition in MRI, it is impossible for both resolutions to be high at the same time.

Therefore, much effort is devoted to using compressed sensing (CS) in MRI. In MRI, the images are acquired in their Fourier domain (also termed k-space). CS comes into play naturally by under-sampling of the k-space (sampling below the Nyquist rate). The k-space sampling trajectories used include: cartesian sampling [6], radial sampling [7] (including the flexible golden-angle technique [8]) and spiral trajectories [9].

Good quality of reconstruction is strongly dependent on good a priori knowledge of the signal. Many CS reconstruction techniques applied to DCE-MRI use basic formulations of single priors, like the total variation (TV) in the spatial [8] or the temporal [10] domain or the wavelet transform in the spatial and/or the temporal domains [6]. The assumption that different tissues have different but consistent perfusion characteristics is usually mathematically described by the low-rank property of the so-called Casorati matrix, which is an image sequence reshaped such that each image in time forms a column vector [11, 12].

More sophisticated approaches in DCE-MRI combine several priors. Article [13] assumes that the Casorati matrix is low-rank and sparse in the spectral domain (row-by-row spectra). A more efficient approach [14] regards the data as the sum of a low-rank component and a component sparse in the spectral domain (L+S model). Superior results have been achieved by regularization via low-rank penalty block-by-block, like in [15, 16].

In the present article, we propose to use the sum of locally low-rank matrix and a component which is sparse in the spectral domain (local L+S model) instead of the (global) L+S model in [14]. We show that we can achieve better signal-to-noise ratio (SNR) with our local L+S model than when using global L+S model. We compare this approach with a model using locally low-rank and component sparse in the spectral domain simultaneously (locally L&S model) as presented in [16].

2 Materials and methods

To work with perfusion data, image sequences are reformatted to the so-called Casorati matrix [11], where each column of this matrix represents a single image in one temporal phase. Such a matrix is used in all models mentioned below.

2.1 Locally low-rank and sparse matrix model (local L&S model)

The locally L&S model [16] utilizes the fact that perfusion curves have similar time courses in some space regions and have a sparse row spectrum. The similar

time-dependency of perfusion curves in each tissue of desired data reconstruction $\mathbf{M}$ is enforced by assuming a low rank of non-overlapping blocks of matrix $\mathbf{M}$ (with a few non-zero singular values in each block) and a sparse row spectrum with a few non-zero elements. Matrix $\mathbf{M}$ is of size $N_1N_2 \times N_\mathrm{f}$, where N_1, N_2 represent the size of each image/frame and N_f is their overall number. The reconstruction can be achieved by solving the following convex optimization problem:

$$\min_{\mathbf{M}} \frac{1}{2}\|E\mathbf{M} - \mathbf{d}\|_\mathrm{F}^2 + \lambda_L \sum_{i=1}^{N_\mathrm{b}} \|B_i\mathbf{M}\|_* + \lambda_S \|T\mathbf{M}\|_1 , \tag{1}$$

where T is the operator of 1D Fourier transform applied to the matrix rows, E is the under-sampled 2D Fourier transform for each image (representing the measurement process), $\mathbf{d}$ is the under-sampled (acquired) data in k-space, and λ_L, λ_S are suitable regularization parameters. B_i is an operator choosing the block i out of the entire matrix, and N_b is the number of blocks. The quadratic term is the data fidelity term, $\|\mathbf{M}\|_*$ is the nuclear norm, which is the sum of singular values of $\mathbf{M}$ (enforces low-rank), and $\|T\mathbf{M}\|_1$ is the ℓ_1-norm, which is the sum of absolute values of entries in $T\mathbf{M}$ (enforces sparsity of perfusion curves in the Fourier domain).

2.2 Low-rank and sparse matrix decomposition (global L+S model)

In the context of perfusion MRI, Low-Rank and Sparse Matrix Decomposition (L+S model) was first introduced in [14]. Unlike the L&S model (either local or global), which aims at promoting low-rank and spectral-domain sparsity of the solution simultaneously, the L+S model aims to compose the desired reconstruction matrix as a sum of low-rank matrix $\mathbf{L}$ and matrix $\mathbf{S}$ with sparse row spectrum, i.e. in this model the desired reconstruction is $\mathbf{M} = \mathbf{L} + \mathbf{S}$. This decomposition can be obtained by solving the following convex problem:

$$\min_{\mathbf{L},\mathbf{S}} \frac{1}{2}\|E(\mathbf{L}+\mathbf{S}) - \mathbf{d}\|_\mathrm{F}^2 + \lambda_L \|\mathbf{L}\|_* + \lambda_S \|T\mathbf{S}\|_1 . \tag{2}$$

2.3 Locally low-rank and sparse matrix decomposition (local L+S model)

In [15, 16], the locally low-rank constraint is used instead of the (global) low-rank and it can improve the quality of desired reconstruction data if applied to areas with similar perfusion curves. We propose using this locally low-rank prior in the previously introduced L+S model instead of using the global low-rank of matrix $\mathbf{L}$. The local L+S model can be formulated as

$$\min_{\mathbf{L},\mathbf{S}} \frac{1}{2}\|E(\mathbf{L}+\mathbf{S}) - \mathbf{d}\|_\mathrm{F}^2 + \lambda_L \sum_{i=1}^{N_\mathrm{b}} \|B_i\mathbf{L}\|_* + \lambda_S \|T\mathbf{S}\|_1 . \tag{3}$$

A crucial question is choosing the appropriate size of the blocks in order to capture areas with similar perfusion parameters and improve the reconstruction as will be shown in the following.

3 Experimental results

3.1 Perfusion phantom

For the purpose of simulation, we have created a perfusion phantom using Matlab. We have utilized the modified Shepp-Logan phantom [17], which simulates a brain slice, see Fig. 1. We use a perfusion phantom of 100×100 px $\times 100$ time points in size. The perfusion curves assigned to clearly separated areas of the phantom share the same behaviour in time, following the log-normal model [3]. At every time instant, the k-space values have been perturbed by additive Gaussian noise with a standard deviation of 0.05 to simulate the measurement noise. This model is simplified but it allows us to accurately compare the behaviour of methods.

To capture perfusion data, we use radial trajectories, where random slopes of halflines starting at the origin of k-space are used independently for each time frame.

Fig. 1. Single temporal frame of perfusion phantom (arrows mark areas in which reconstruction of perfusion parameters using different methods is further compared).

3.2 Under-sampled perfusion data reconstruction

For under-sampled perfusion-phantom data, three types of reconstruction were performed, based on: local L&S model (1), global L+S model (2) and local L+S model (3). The respective optimization problems were solved using the proximal gradient method [18]. Non-overlapping square blocks of different sizes were used for local methods. The parameters λ_L, λ_S were empirically chosen (dependent on the method used, size of blocks and resolution, see Figs 2 and 3) such that the reconstruction gave the highest possible SNR. In all cases, algorithms were stopped when the relative change in the solution was less than 10^{-5}.

Reconstructions of perfusion curves were compared for the global and local L+S models, using different sizes of the blocks and different percentages of measured coefficients, see Fig. 2. Partitioning into blocks brought an increase in the

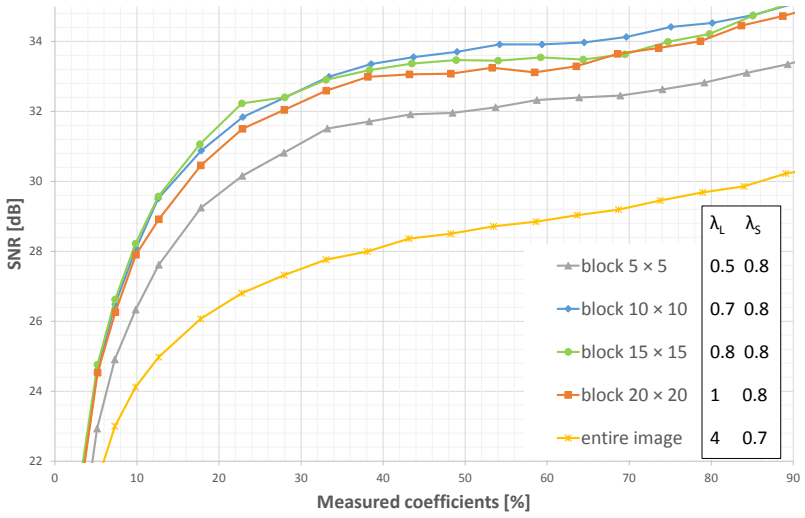

Fig. 2. Comparison of global and local L+S models — dependency of SNR on percentage of measured coefficients.

SNR. It can be seen that block size affects the reconstruction quality. The optimal block size depends on the contents of the image used — better performance is achieved for blocks small enough to include only a tissue with similar perfusion parameters but large enough to regularize sufficient area. For the perfusion phantom, the optimal block sizes were 10×10 and 15×15, the latter valid for the strongly under-sampled acquisition.

A comparison of the local L+S model (for an optimal block size of 10×10) and the local L&S model for various block sizes is shown in Fig. 3. It can be seen that the local L+S model has even a better SNR than when using the optimal block size (10×10 or 15×15) in the local L&S model.

In Fig. 4, the reconstructed perfusion curves (from 35 % of coefficients) in different regions (marked by red arrows in Fig. 1) are compared for global and local L+S model (with the reference perfusion phantom curves), local L+S model and local L&S model respectively. Usually, the local L+S model better follows the shape of perfusion curves but it is smoother than in the case of the global L+S model and local L&S model. Notice also that non-perfused tissue (Fig. 4(c)) is also better approximated by the local L+S model than by the others.

To have an idea of the speed of convergence, the reconstruction from 35 % of measured coefficients, using blocks 10×10, takes about 24 iterations (30 s) using the L&S model, and 163 iterations (105 s) using the L+S model. The local L+S converges faster than the global L+S model because the SVD (singular value decompositon) is computed on much smaller matrices.

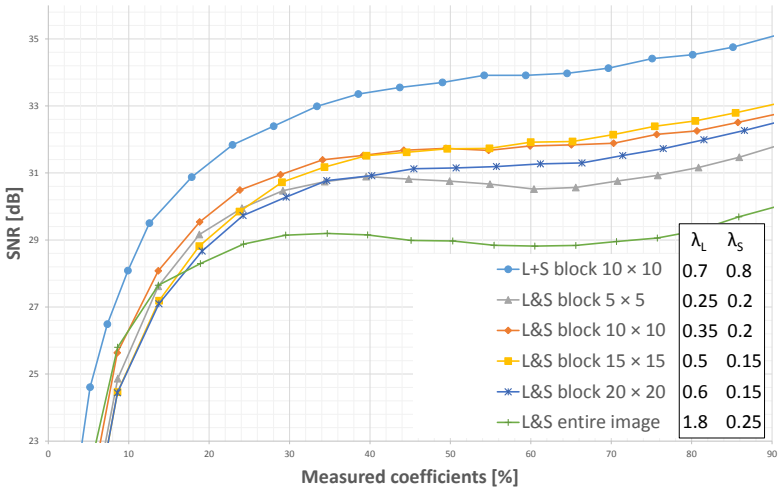

Fig. 3. Comparison of local L+S model and local L&S models — dependency of SNR on percentage of measured coefficients.

4 Conclusion

The use of advanced pharmacokinetic models in magnetic resonance perfusion imaging is a promising method that allows estimating of additional highly relevant perfusion parameters. However, it requires high spatio-temporal resolution, which is not possible when using the classic acquisition in MRI. The article proposes using a local L+S model to reconstruct under-sampled perfusion data. The results obtained on a perfusion phantom indicate that the proposed local L+S model recovers more accurate perfusion curves than the global L+S model and the local L&S model, even in the highly under-sampled regime.

Acknowledgement The authors thank M. Šorel for careful reading of the manuscript. The research was supported by the Ministry of Education, Youth, and Sports of the Czech Republic (project No. LO1212), by the SIX project registration number CZ.1.05/2.1.00/03.0072, and by the Czech Science Foundation grant no. GA15-12607S.

References

1. A. Jackson, D. L. Buckley, and M. Parker. *Dynamic Contrast-Enhanced Magnetic Resonance Imaging in Oncology*. Springer, Berlin, 2005.
2. M. Mézl, R. Jiřík, and V. Harabiš. Acquisition and data processing in ultrasound perfusion analysis. In *New trends in biomedical engineering*, pages 44–51. Brno University of Technology, 2013. In Czech.
3. V. Harabiš, R. Kolář, M. Mézl, and R. Jiřík. Comparison and evaluation of indicator dilution models for bolus of ultrasound contrast agents. *Physiological Measurement*, 34:151–162, 2013.

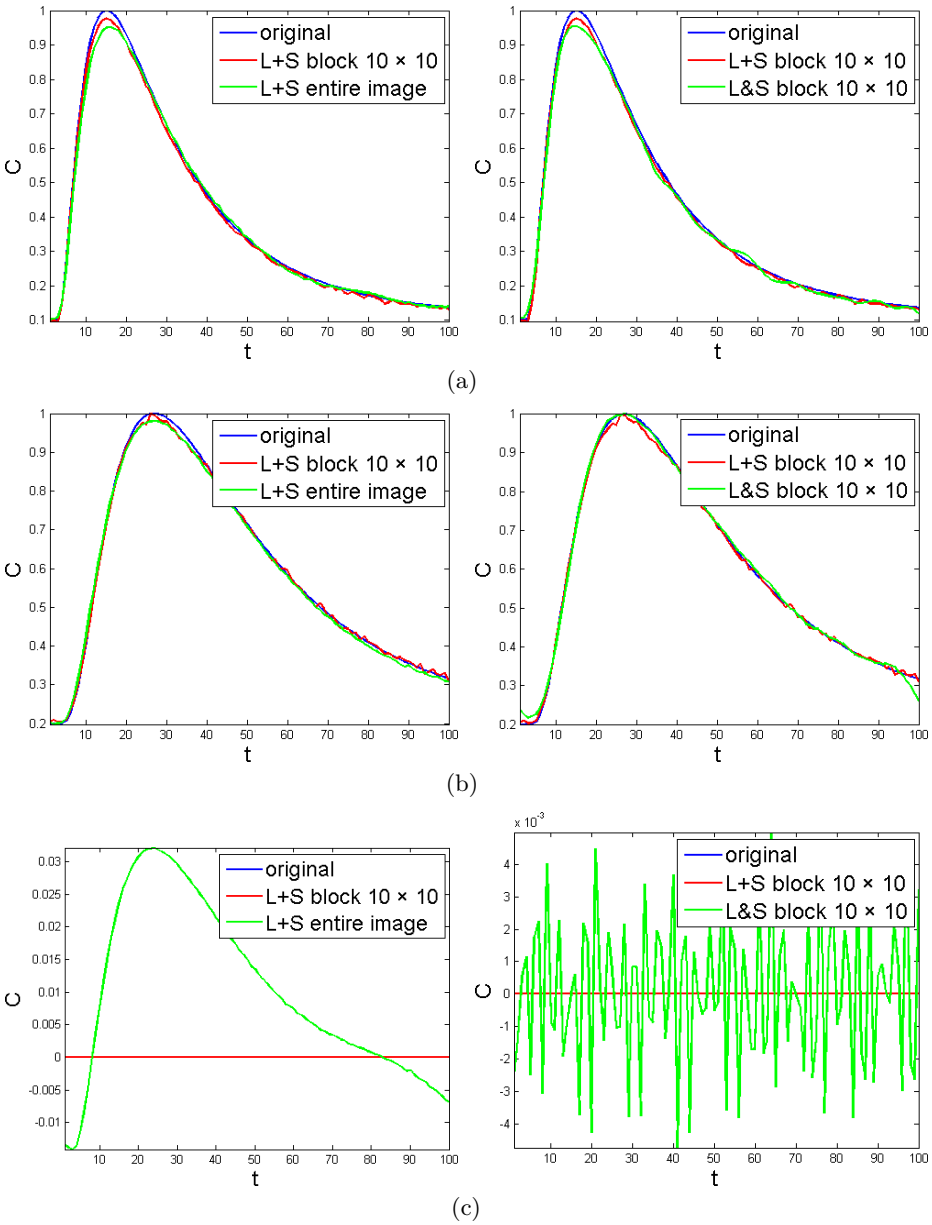

Fig. 4. Reconstruction of perfusion curves (from 35 % of the Fourier coefficients) in different regions (marked by red arrows in Fig. 1) using global and local L+S model (left) and local L+S and local L&S model (right), the last pair represents non-perfused tissue (the blue line, i.e. the original curve, is hidden under the red line, representing the local L+S model).

4. Michal Bartoš. *Advanced signal processing methods in dynamic contrast enhanced magnetic resonance imaging*. Doctoral thesis, Brno University of Technology, 2014.
5. S P Sourbron and D L Buckley. Tracer kinetic modelling in MRI: estimating perfusion and capillary permeability. *Physics in medicine and biology*, 57(2):R1–33, January 2012.
6. SoHyun Han, Jeffrey L. Paulsen, Gang Zhu, Youngkyu Song, SongI Chun, Gyunggoo Cho, Ellen Ackerstaff, Jason A. Koutcher, and HyungJoon Cho. Temporal/spatial resolution improvement of in vivo DCE-MRI with compressed sensing-optimized FLASH. *Magnetic Resonance Imaging*, 30(6):741–752, 2012.
7. Kai Tobias Block, Martin Uecker, and Jens Frahm. Undersampled radial MRI with multiple coils. Iterative image reconstruction using a total variation constraint. *Magnetic Resonance in Medicine*, 57(6):1086–1098, 2007.
8. Z. Li, B. P. Berman, M. I. Altbach, et al. Highly accelerated 3D dynamic imaging with variable density golden angle stack-of-stars sampling. In *Proc. Intl. Soc. Mag. Reson. Med. 21*, page 3797, 2013.
9. Juan M. Santos, Charles H. Cunningham, Michael Lustig, Brian A. Hargreaves, Bob S. Hu, Dwight G. Nishimura, and John M. Pauly. Single breath-hold whole-heart MRA using variable-density spirals at 3T. *Magnetic Resonance in Medicine*, 55(2):371–379, 2006.
10. K. Sungheon, L. Feng, L. Moy, et al. Highly accelerated golden-angle radial acquisition with joint compressed sensing and parallel imaging reconstruction for breast DCE-MRI. In *Proc. Intl. Soc. Mag. Reson. Med. 21*, page 1468, 2012.
11. N. Zhang, G. Song, W. Liao, et al. Accelerating dynamic contrast-enhanced MRI using K-T ISD. In *Proc. Intl. Soc. Mag. Reson. Med. 21*, page 4221, 2012.
12. Haoyu Wang, Yanwei Miao, Kun Zhou, Yanming Yu, Shanglian Bao, Qiang He, Yongming Dai, Stephanie Y. Xuan, Bisher Tarabishy, Yongquan Ye, and Jiani Hu. Feasibility of high temporal resolution breast DCE-MRI using compressed sensing theory. *Medical physics*, 37(9):4971–4981, September 2010.
13. S.G. Lingala, Yue Hu, E. DiBella, and M. Jacob. Accelerated dynamic MRI exploiting sparsity and low-rank structure: k-t SLR. *Medical Imaging, IEEE Transactions on*, 30(5):1042–1054, May 2011.
14. Ricardo Otazo, Emmanuel Candes, and Daniel K. Sodickson. Low-rank plus sparse matrix decomposition for accelerated dynamic MRI with separation of background and dynamic components. *Magnetic Resonance in Medicine*, 73(3):1125–1136, 2015.
15. Tao Zhang, Joseph Y. Cheng, Aaron G. Potnick, Richard A. Barth, Marcus T. Alley, Martin Uecker, Michael Lustig, John M. Pauly, and Shreyas S. Vasanawala. Fast pediatric 3D free-breathing abdominal dynamic contrast enhanced MRI with high spatiotemporal resolution. *Journal of Magnetic Resonance Imaging*, 41(2):460–473, 2015.
16. Tao Zhang, Marcus Alley, Michael Lustig, Xiaodong Li, John Pauly, and Shreyas Vasanawala. Fast 3D DCE-MRI with sparsity and low-rank enhanced SPIRiT (SLR-SPIRiT). *Proceedings of the 21st Annual Meeting of ISMRM, Salt Lake City, Utah, USA*, page 2624, 2013.
17. Lawrence A. Shepp and B. F. Logan. The Fourier reconstruction of a head section. *IEEE Transactions on Nuclear Science*, 21:21–43, 1974.
18. P.L. Combettes and J.C. Pesquet. Proximal splitting methods in signal processing. *Fixed-Point Algorithms for Inverse Problems in Science and Engineering*, pages 185–212, 2011.